# Synthesis of High-Quality $AgSbSe_2$ and $AgBiSe_2$ Nanocrystals with Antimony and Bismuth Silylamide Reagents

Adita Das[†], Bo Hsu[‡], Armen Shamirian[†], Zheng Yang[‡], Preston T. Snee[†*]

†Department of Chemistry, University of Illinois at Chicago, 845 West Taylor Street, Chicago, IL 60607-7061 USA

‡ Department of Electrical and Computer Engineering, University of Illinois at Chicago, Chicago, IL 60607, USA

*KEYWORDS. Dimetal chalcogenide, quantum dot, nanocrystal, thermoelectric*

**ABSTRACT:** Silver dimetal chalcogenides (Ag-V-$VI_2$) are ternary semiconductors that have potential alternative energy applications due to their optimal band gaps and large extinction coefficients. The synthesis of these materials is challenging due to the lack of effective pnictide precursors. We report the use of tris[N,N-bis-(trimethylsilyl)amido]antimony ($Sb[N(SiMe_3)_2]_3$) and tris[N,N-bis-(trimethylsilyl)amido]bismuth ($Bi[(N(SiMe_3)_2]_3$) to synthesize nanocrystalline $AgSbSe_2$ and $AgBiSe_2$ quantum dots. The use of these reagents results in the creation of high quality nanomaterials with good crystallinity and narrow size distributions. Furthermore, electrical measurements on monolithic pellets of processed $AgSbSe_2$ and $AgBiSe_2$ nanomaterials demonstrate linear current-voltage behavior at room temperature, which indicates potential for use in electrical applications.

## INTRODUCTION

The development of advanced semiconductor materials is important to address the problems associated with the non-sustainable consumption of environmental resources due to worldwide overpopulation. In this regard, semiconductors can be used to create solar panels and catalysts for alternative energy generation, as well as efficient lighting systems and "smart windows" for energy conservation.[1, 2] Furthermore, semiconductor thermoelectric materials can generate power from the excess heat that is the byproduct of processes such as fossil fuel combustion.[3] Many of these examples were not realized with bulk materials that have well-defined physical properties. Such limitations engender only a certain level of efficacy for use in applications. It is necessary to build advanced materials on the nanoscale to overcome this deficit, due to the ability to tune electronic properties with size.[4] Bottom-up chemical syntheses have been used to create colloidal semiconductor nanocrystals (NCs, also known as quantum dots) that have size dependent properties engendered through quantum confinement.[4, 5] Research on quantum dots have overwhelmingly centered on II-VI (i.e. CdE, E=S, Se, Te) NCs, while other material systems such as pnictides (group V) have not been examined as extensively. This is due to the fact that the syntheses of pnictide nanomaterials are intricate and dangerous and there are few low-cost commercially available non-pyrophoric precursors.[6-9]

Among pnictides, environmentally benign I-V-$VI_2$ semiconductor nanocrystals are an emerging class of materials due to their NIR band gaps, large absorption coefficients, and excellent electronic properties.[10, 11] Dimetal chalcogenides have utility for photovoltaic and thermoelectric applications, making them promising alternatives for thermoelectric PbTe.[12, 13] There are several examples of the synthesis of copper-based I-V-$VI_2$ quantum dots, whereas silver-based nanomaterials such as $AgBiS_2$, $AgSbS_2$, $AgSbSe_2$, and $AgBiSe_2$ are less common.[14-16] The majority of reports on their syntheses used high temperature (~1000 K) solid state reactions that required long annealing times. Furthermore, the products were reported to have poor crystallinity and significant polydispersity. Colloidal preparation of $AgSbSe_2$ has been reported to yield significantly more monodisperse materials.[17]

Our group recently demonstrated the use of an efficient, versatile, and most importantly non-pyrophoric arsenic precursor, $AsCl[(N(SiMe_3)_2]_2$,[18, 19] to synthesize a variety of semiconductor quantum dots and rods.[9] Herein we report the utility of additional silylamide-ligated pnictides, specifically tris[N,N-bis(trimethylsilyl)amido]antimony ($Sb[(N(SiMe_3)_2]_3$) and tris[N,N-bis(trimethylsilyl)amido]bismuth ($Bi[(N(SiMe_3)_2]_3$),[8, 20, 21] to synthesize silver dimetal chalcogenide quantum confined nanocrystals. These reagents were prepared via a simple one step metathesis reaction between the pnictide halide ($SbCl_3$/$BiCl_3$) and $Li[N(SiMe_2)_2]_3$ as summarized in Scheme 1; further details and characterizations are in the supporting information. Both compounds are stable and relatively easy to handle due to the fact that they are solid-state reagents. Furthermore, they are soluble in a variety of organic solvents. As a result, they have been successfully applied to the syntheses of monodisperse, crystalline $AgSbSe_2$ and $AgBiSe_2$ nanoparticles using high-temperature colloidal methods. Specifically, $AgSbSe_2$ nanoparticles were generated via hot injection method, while the optimal strategy for synthesizing $AgBiSe_2$ NCs used a 'heat-up' procedure.

The most interesting discovery concerns the fact that no reducing agents were required to activate either $Sb[(N(SiMe_3)_2]_3$ nor $Bi[(N(SiMe_3)_2]_3$, as was necessary for the

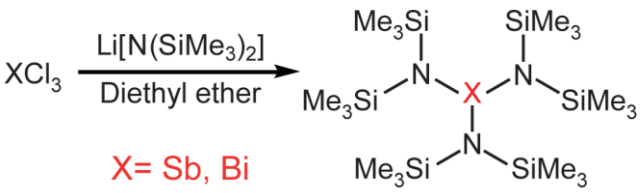


**Scheme 1. Synthesis of tris[N,N-bis(trimethylsilyl)amido]antimony, $Sb[(N(SiMe_3)_2]_3$ and tris[N,N-bis(trimethylsilyl)amido]bismuth, $Bi[(N(SiMe_3)_2]_3$.**

synthesis of arsenide and antimonide nanomaterials in our earlier study and by Liu et al.[8] In fact, inclusion of a reducing agent resulted in a bivariate distribution of nanoparticle sizes as discussed in the supporting information, see Figure S11. This is likely due to separate nucleation events, where some materials were generated by the reducing agent while others resulted via heat activation. The results of each individual system have been reported in 'Results and Discussion section' followed by electrical measurement data on monolithic pellets of the materials.

## EXPERIMENTAL

**Materials:** Bismuth chloride ($BiCl_3$, 99.9%) and selenium shot (99.5%) were purchased from Strem Chemicals. Hexane (anhydrous, 95%) and antimony chloride ($SbCl_3$, 99%) were purchased from Alfa Aesar. Oleic acid (OA, 90%), oleylamine (OLA, 98%), lithium bis(trimethylsilyl)amide ($Li[N(Si(Me)_3)_2]$, 97%), 1-dodecanethiol (DDT, 98%), ethanol (>99.5%), silver(I) chloride (AgCl, 99.995%) and sodamide ($NaNH_2$, 95%) were obtained from Sigma-Aldrich. Diethyl ether (purchased from VWR) was sparged with argon and dried using a Glass Contour Solvent System from Pure Process Technology, LLC. Antimony chloride, bismuth chloride, lithium bis(trimethylsilyl)amide were stored and handled in an inert atmosphere glove box. Oleic acid was recrystallized according to the procedures in ref. 22, while other chemicals were used without further purification.

**Synthesis of $Sb[(N(SiMe_3)_2]_3$:** The procedure developed by Liu et al.[8] was used to synthesize tris[N,N-bis(trimethylsilyl)amido]antimony. The preparation is based on a metathesis reaction between antimony chloride and lithium bis(trimethylsilyl)amide. First, 760 mg $SbCl_3$ (3.33 mmol) was dissolved in a mixture of dry ether (15 mL) and THF (3 mL), and was slowly added dropwise to a stirring solution of 1.7 g lithium bis(trimethylsilyl)amide (10 mmol) in ether (10 mL) at 0 °C under an inert $N_2$ atmosphere. The solution became white in color and turbid during the addition, and was kept stirring at 0 °C for an additional hour. The resulting white solution was warmed to room temperature and kept overnight. Afterwards, the solution was filtered using a glass fritted funnel and the solvents were removed under reduced pressure, resulting in a pale yellow colored $Sb[(N(SiMe_3)_2]_3$ product. The product was recrystallized from a saturated hexane solution, resulting in the white solid product $Sb[(N(SiMe_3)_2]_3$, yield ~ 80%. The purity of the product was determined via NMR; $^1H$ NMR (25 °C, $CDCl_3$, 400MHz) 0.29 (s); see the spectrum in Figure S1. The reagent was stored in a -80 °C freezer in a sealed vial.

**Synthesis of $Bi[N(SiMe_3)_2]_3$:** The procedure developed by Carmalt et al.[20] was used to synthesize tris[bis(trimethylsilyl)amide]bismuth. The preparation is based on a metathesis reaction between bismuth chloride and lithium bis(trimethylsilyl)amide. First, 1.0 g $BiCl_3$ (3.17 mmol) was added into a round bottom flask under a dry nitrogen atmosphere. Next, 20 mL of dry ether and 5 mL THF were added to the flask, which was maintained the temperature at 0°C. Next, 1.6 g lithium bis(trimethylsilyl)amide (9.51 mmol) dissolved in 15 mL of dry ether was added dropwise into the $BiCl_3$ solution. The resulting mixture became yellow in color and turbid. It was kept stirring at 0 °C for another hour and then slowly warmed to room temperature. Afterwards, the solution was filtered through a glass fritted funnel under an inert $N_2$ atmosphere and the solvents were removed under reduced pressure. Finally, the product was recrystallized from a saturated toluene solution, resulting in a yellow solid $Bi[N(SiMe_3)_2]_3$ product, yield ~ 90%. The purity of the product was determined via NMR; $^1H$ NMR (25 °C, $CDCl_3$, 400MHz) 0.36 (s); see the spectrum in Figure S1. The reagent was stored in glove box covered with aluminum foil.

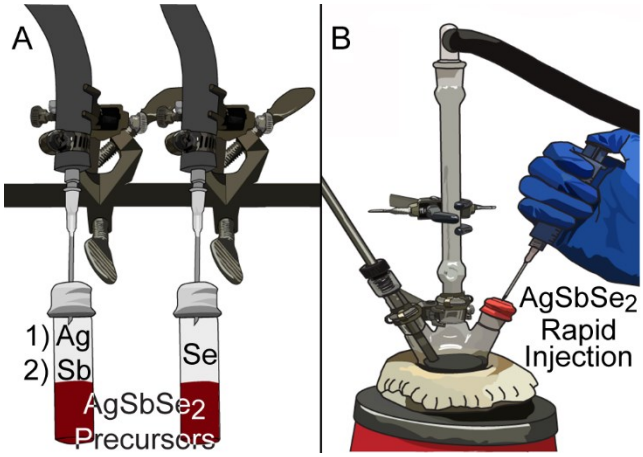


**Scheme 2. (a) Synthesis of $AgSbSe_2$ NCs begins with degassing the Ag and Sb reagents separately followed by (b) sequential rapid injection of Sb and Ag precursors. Note that $AgBiSe_2$ NCs are prepared by heating up the solvent and precursors in a single reaction vessel.**

**Synthesis of $AgSbSe_2$ nanoparticles:** 10 mL of oleylamine was added into a three-neck round-bottom flask and degassed under vacuum at 110 °C for 2 hours. In a 7 mL septa-covered vial labeled "A", 5 mL of oleylamine and 1 mL of oleic acid were added and were subsequently degassed under vacuum. Next, 85 mg (0.5 mmol) of $AgNO_3$ was added to this vial, which was kept stirring at 80 °C under an $N_2$ atmosphere until the solid dissolved completely. Next, the vial was cooled to 40 °C, and 300 mg (0.5 mmol) of $Sb[(N(SiMe_3)_2]_3$ dissolved in 0.5 mL toluene was added while maintaining the nitrogen atmosphere. In a separate vial labeled "B", 98 mg of selenium (1.25 mmol) was dissolved in a mixture of 0.5 mL oleylamine and 0.5 mL dodecanethiol. Afterward, the oleylamine in the three neck round bottomed flask was heated to 180°C. The solution in vial "A" was injected into the flask at 180 °C followed by an injection of the solution in vial "B". This resulted in the formation of a dark brown coloration. The solution was maintained at 180 °C for 2-3 mins. Afterwards, the heating mantle was removed and the solution was allowed to cool to room temperature. The sample was stored under an inert $N_2$ atmosphere in a glovebox.

**Synthesis of $AgSbSe_2$ nanoparticles in presence of a reducing agent:** 10 mL of oleylamine and 85 mg (0.5 mmol) of $AgNO_3$ were added into a three-neck round bottom flask and degassed at 110 °C for 2 hours. At the same time, 300 mg (0.5 mmol) of $Sb[(N(SiMe_3)_2]_3$ was dissolved in 0.5 mL toluene and 98 mg of selenium (1.25 mmol) was dissolved in a mixture of 0.5 mL oleylamine and 0.5 mL dodecanethiol. The oleylamine in three-neck round bottom flask was cooled to 30°C and 0.9 mL of 1 M lithium triethylborohydride (0.9 mmol) and $Sb[(N(SiMe_3)_2]_3$ solution in toluene was injected into the flask at 30 °C followed by an addition of the solution of selenium precursor. This resulted in the formation of a black colored suspension, which was then slowly heated to 180°C and maintained at 180 °C for another 10 mins. Afterwards, the heating mantle was removed and the solution was quickly allowed to cool to room temperature. The sample was stored under an inert atmosphere in a glovebox. A similar procedure was employed to synthesize $AgBiSe_2$ NCs, however the poor size distribution

of $AgSbSe_2$ nanoparticles obtained using this procedure caused us to abandon the use of reducing agents.

**Synthesis of $AgBiSe_2$ nanoparticles:** 10 mL of oleylamine and 85 mg (0.5 mmol) of $AgNO_3$ were added into a three-neck round bottom flask and degassed at 110 °C for 2 hours. At the same time, 345 mg (0.5 mmol) of $Bi[(N(SiMe_3)_2]_3$ was dissolved in 0.5 mL toluene and 98 mg of selenium (1.24 mmol) was dissolved in a mixture of 0.5 mL oleylamine and 0.5 mL dodecanethiol. Afterward, the oleylamine in three-neck round bottomed flask was cooled to 30°C and the $Bi[(N(SiMe_3)_2]_3$ solution was injected into the flask at 30 °C followed by the selenium precursor solution. This resulted in the formation of a black colored suspension. The solution was slowly heated to 200°C and maintained at 200 °C for an additional 10 mins. Afterwards, the heating mantle was removed and the solution was allowed to cool to room temperature. The sample was stored under an inert $N_2$ atmosphere in a glovebox.

**Surface ligand treatment and pellet formation:** The following procedure was applied to both $AgSbSe_2$ and $AgBiSe_2$ samples in an identical manner. First, 800 mg of a sample was precipitated with an ethanol / isopropanol mixture and centrifuged. Next, the material was dispersed into 10 mL chloroform to which 10 mL of 0.01 M sodamide ($NaNH_2$) solution in ethanol was subsequently added. Afterwards, the sample was repeatedly washed with isopropanol and chloroform. Finally, a fine powder of nanocrystals was obtained after drying under vacuum. After ligand treatment, 500 mg of each fine powder were pressed into form a pellet under an applied pressure of 7.4 metric tons (~ 16000 lbs.). This procedure is outlined in Figure S6 of the supporting information.

**Characterization:** For characterization, a small quantity of each sample was precipitated with ethanol and centrifuged to remove impurities. The precipitate was then redispersed in dry hexane and characterized by optical, X-ray photoelectron (XPS), and X-ray diffraction (XRD) spectroscopies. Absorption measurements were performed with a Perkin Elmer LAMBDA 1050 UV/Vis-NIR spectrophotometer. XPS analyses were performed on a Kratos Axis 165 using a monochromatic Al Kα source operating at 12 kV and 10 mA to produce an X-ray power of 120 W. Spectra were collected with a photoelectron takeoff angle of 90° from the sample surface plane, in energy steps of 0.1 eV, and a pass energy of 20 eV for all elements. All spectra were referenced to the C1s binding energy (284.8 eV). X-ray diffraction studies were performed on a D8 Advance ECO Bruker XRD diffractometer using monochromatized Cu Kα (λ= 1.54056 Å) radiation. Transmission electron microscopy (TEM) measurements were performed using a JEOL JEM-3010 operating at 300 keV. A 300 mesh gold grid was used for TEM analysis. $^1$H NMR spectra were recorded using Bruker Avance DRX 400 NMR spectrometer.

**Electrical Measurement:** Electrical measurement [current-voltage (I-V) characteristics] of the $AgSbSe_2$ and $AgBiSe_2$ quantum dot pellets were measured using a Keithley 2400 source meter at room temperature. Copper wires were soldered using indium on various locations of $AgSbSe_2$ and $AgBiSe_2$ quantum dot pellets as electrode contacts for I-V measurements.

**Quantum Chemical Modeling:** All species were modeled with Density Functional Theory, specifically B3LYP,[23, 24] using the Gaussian '09 package.[25] The LANL2DZ basis set corresponding effective core potentials were employed.[26] The antimony substrate $Sb[(N(SiMe_3)_2]_3$ was modeled using $Sb[(N(SiH_3)_2]_3$, while a silver-oleic acid was modeled using neutral $Ag\text{-}O_2C_2H_3$. All geometry optimizations, including saddle points, were characterized with frequency analyses. Saddle points were examined using intrinsic reaction coordinate analysis. Zero point vibrational corrections were added to the energies. GaussView was used to visualize the results.[27]

## RESULTS AND DISCUSSION

**Silver antimony selenide ($AgSbSe_2$):** $AgSbSe_2$ is a narrow indirect bandgap (0.58 eV) semiconductor with intrinsic p-type conductivity. It is a promising candidate for thermoelectric applications due to its high Seebeck coefficient, low thermal conductivity, and good stability.[28-31] Furthermore, it is considered to be an excellent photovoltaic material due to its strong absorption.[30-32]

The synthesis of $AgSbSe_2$ NCs was studied via the hot injection method according to the following:

$AgNO_3 + Sb[(N(SiMe_3)_2]_3 + Se(\text{oleylamine/dodecanethiol}) \rightarrow AgSbSe_2$

To this end, two separate solutions of precursors were co-injected into oleylamine at 180°C as represented in Scheme 2. One contained the antimony and $AgNO_3$ reagents dissolved in an oleylamine and oleic acid mixture. This was done to enhance the crystallinity of the $AgSbSe_2$ nanoparticle products under the rational that oleic acid stabilizes the hard Sb (+3) ions while oleylamine stabilizes the soft Ag (+1) ions. The sequence of addition of precursors during the preparation of the antimony and silver injection solution is important as the product does not have pure crystallinity if the protocol is not followed exactly. The second solution that was co-injected contained selenium dissolved in oleylamine.

A variety of characterization results are shown in Figure 1, all of which demonstrate the synthesis of ~9 nm crystalline nanoparticles of $AgSbSe_2$. XPS results shown in Figure S2 confirm the stoichiometry of the products. The crystal phase of the nanoparticles is consistent with characteristic pattern of the cubic phase of $AgSbSe_2$. The absorption spectrum in Figure S3 is featureless; however, the absorption onset (~1300 nm) is greater than the bulk bandgap. This is potentially due to quantum confinement, which affords the possibility for manipulation of the properties of artificial solids that incorporate these materials. There are important differences to note between the results of this study and previous demonstrations of $AgSbSe_2$ material synthesis. For example, the preparation of nanocrystalline silver antimony dichalcogenide using solid state conditions results in polydisperse samples.[32] As such, colloidal methods are preferred, and indeed Lin et al. first demonstrated homogeneous 7-17 nm $AgSbSe_2$ NCs via the rapid injection procedure using $SbCl_3$ as the pnictide source.[17] The use of $Sb[(N(SiMe_3)_2]_3$ as presented in this report created a similar small size of NCs; however, our protocol requires ~1/10$^{th}$ the quantity of precursors. Furthermore, the use of $SbCl_3$ results in an initial bimodal size distribution that grew into a monodisperse population over 30 min.[17] In contrast, we observed a reasonably monodisperse $AgSbSe_2$ NC population within 3 minutes of injection, which indicates fast homogeneous nucleation and growth.

These observations lead us to conclude that $Sb[(N(SiMe_3)_2]_3$ has enhanced reactivity compared to $SbCl_3$. To study this further, the potential energy surfaces of a silver-acid complex with the corresponding pnictide precursors were calculated using DFT as shown in Figures S4 and S5. A ligand exchange reaction to form an antimony-organic acid intermediate was studied as a potential first step. It was found that $SbCl_3$

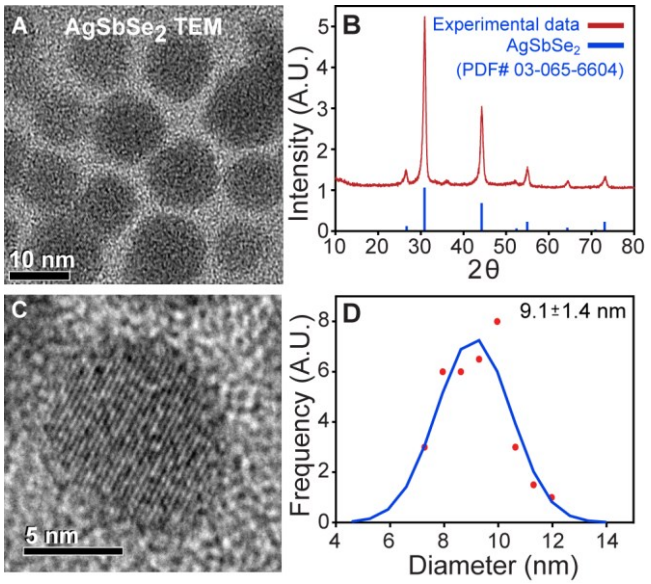


**Figure 1**. (a) TEM image of $AgSbSe_2$ nanoparticles. (b) X-ray diffraction pattern of $AgSbSe_2$ NCs confirm their structure and crystallinity. (c) High resolution TEM image of crystalline $AgSbSe_2$ showing lattice fringes. (d) Size distribution of $AgSbSe_2$ dots.

forms a tightly-bound complex with the silver-acetic acid precursor, which results in a significantly uphill reaction barrier for subsequent ligand exchange. However, the same interaction with $Sb[(N(SiH_3)_2]_3$ (a model compound for antimony silylamide) is much weaker and the overall reaction is less endothermic. These results are consistent with the experimental findings, and lead us to conclude that the effect of the pnictide ligand is significant. In this case, the ability of antimony to participate in chemical transformations that result in the formation of $AgSbSe_2$ NCs is enhanced by the bulky -N(TMS) ligands that prevent the formation of intermediate trap states with silver.

**Silver bismuth selenide ($AgBiSe_2$):** $AgBiSe_2$ is another interesting member of the I-V-$VI_2$ semiconductor family that has excellent thermoelectric properties.[33] At room temperature, it is p-type with a hexagonal phase, and can undergo a structural transition to cubic via a rhombohedral intermediate phase.[34] Both the hexagonal and rhombohedral materials are narrow band gap (~ 0.6 eV) semiconductors, while the high temperature cubic phase behaves like a metal with a high electrical conductivity yet a low thermal conductivity.[14, 34] At present, there is only one other example of the colloidal synthesis of silver bismuth selenide.[33] This rapid injection process required long annealing times that yielded anisotropic nanoparticles, while our heat-up protocol using $Bi[N(SiMe_3)_2]_3$ generated more homogeneous and spherical nanocrystals within ~10 min according to the following:

$AgNO_3 + Bi[(N(SiMe_3)_2]_3 + Se(\text{oleylamine/dodecanethiol}) \rightarrow AgBiSe_2$

We have synthesized $AgBiSe_2$ NCs at 200°C using $Bi[(N(SiMe_3)_2]_3$, $AgNO_3$, and selenium in an oleylamine solution. In contrast to the antimonide system, the rapid injection of precursors resulted in materials with broad and unidentifiable XRD patterns. This prompted the use of a heat-up procedure, which produces significantly cleaner results as shown in Figure 2. The results are consistent with the synthesis of small, ~6 nm diameter crystalline dots, albeit the materials are less monodisperse compared to $AgSbSe_2$ NCs. The crystal phase of the

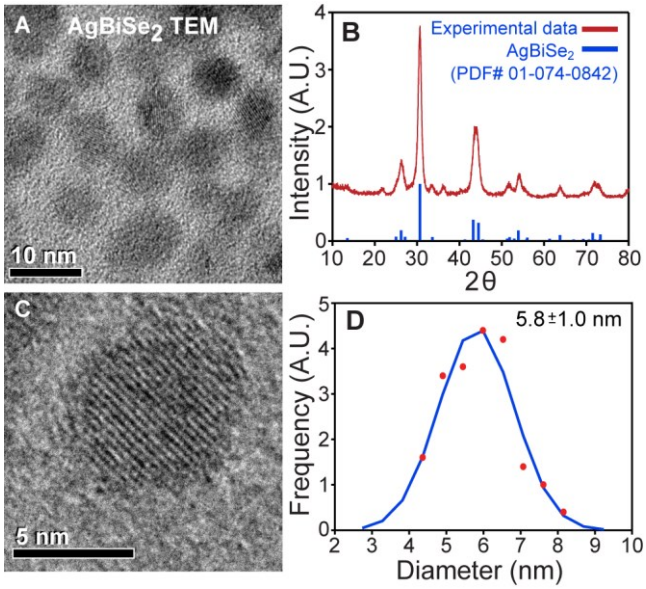


**Figure 2.** (a) TEM image of $AgBiSe_2$ nanoparticles. (b) X-ray diffraction pattern of $AgBiSe_2$ nanoparticles. (c) High resolution TEM image of crystalline $AgBiSe_2$ showing lattice fringes. (d) Size distribution of $AgBiSe_2$ dots.

nanoparticles was confirmed by powder XRD and is consistent with characteristic pattern of the complex hexagonal phase of $AgBiSe_2$. XPS result also confirms the composition of $AgBiSe_2$ nanoparticles although there exists a slight excess of selenium; see Figure S2 of the supporting information. As was observed in the antimonide materials, the absorption spectrum shown in Figure S3 is featureless and has a higher energy onset (~ 1200 nm) compared to the bandgap, which is indicative of quantum confinement effects.

**Electrical measurement:** Room temperature I-V behavior was measured to characterize the electrical conductivity of silver dimetal chalcogenide artificial solids. The materials were precipitated and processed by washing with a sodamide solution. FTIR spectroscopy confirm the removal of the original ligands shown in Figure S7. The resulting $AgSbSe_2$ and $AgBiSe_2$ nanoparticle powders were transformed into 13 mm × 0.9 mm thick pellets in a press. Copper wires were soldered to the surface using indium as electrode contacts as seen in the inset of Figure 3. Also shown are the room temperature two-terminal current-voltage (I-V) plots of the $AgSbSe_2$ and $AgBiSe_2$ quantum dot monoliths. All the I-V measurements demonstrate linear resistive behavior, indicating Ohmic contact nature of the soldered electrodes. Three contact points were used to verify the proper resistance vs. electrode distance behavior as well as confirm good uniformity of the nanomaterials throughout the pellet, see Figure S8. Overall, the conductivity is significantly smaller than bulk materials; furthermore, the bismuth NCs are much lower than the antimony materials despite their similar bulk transport properties.[14] This is likely due to both the smaller size and higher polydispersity of the $AgBiSe_2$ sample, as these factors increase the resistance in solid monoliths of semiconductor nanocrystals.[35] The conductivity of the $AgSbSe_2$ NCs using the method of Lin et al. was reported to be significantly higher than observed here,[17] which may be due to the fact that we did not attempt to thermally anneal the NC pellets.

In conclusion, we have successfully developed a synthetic route to create $AgSbSe_2$ as well as $AgBiSe_2$ nanocrystals using silylamido-based antimony and bismuth precursors. The reaction did not require a reducing agent to activate the pnictide-N

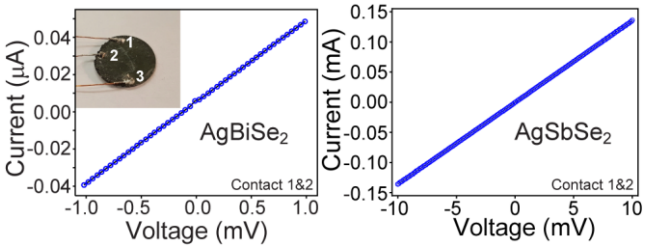


**Figure 3**. I-V measurement of $AgBiSe_2$ and $AgSbSe_2$ monolithic NC pellets (inset). Additional data are presented in the supporting information, see Figure S8.

bond, which is uncommon and results in the synthesis of better materials with enhanced monodispersity and crystallinity. The I-V curves from NC monoliths is indicative of linear resistive behavior which demonstrates their potential for use in electrical devices. These results reveal several paradigms concerning pnictide chemistry as it applies to the synthesis of nanomaterials.

## ASSOCIATED CONTENT

Supporting Information. Additional characterization, including TEM micrographs, and spectroscopic data. This material is available free of charge via the Internet at http://pubs.acs.org.

## AUTHOR INFORMATION

### Corresponding Author

*sneep@uic.edu

### Author Contributions

The manuscript was written through contributions of all authors. All authors have given approval to the final version of the manuscript.

### Funding Sources

The University of Illinois at Chicago.

### Notes

The authors declare no competing financial interests.

## ACKNOWLEDGMENT

We would like to thank Jordi Cabana for assistance with XRD measurements, Mike Plews for assistance with the pellet press, and the Keck Biophysical facilities at Northwestern University for access to UV/Vis/NIR instrumentation. This work was supported by startup funding to PTS from the University of Illinois at Chicago.

## ABBREVIATIONS

NIR, near-Infrared; XRD, X-ray diffraction; XPS, X-ray photoelectron spectroscopy.

## REFERENCES

(1) Kim, G.-H.; García de Arquer, F. P.; Yoon, Y. J.; Lan, X.; Liu, M.; Voznyy, O.; Yang, Z.; Fan, F.; Ip, A. H.; Kanjanaboos, P.; Hoogland, S.; Kim, J. Y.; Sargent, E. H. High-Efficiency Colloidal Quantum Dot Photovoltaics via Robust Self-Assembled Monolayers. *Nano Lett.* **2015**, *15*, 7691-7696.

(2) Llordes, A.; Garcia, G.; Gazquez, J.; Milliron, D. J. Tunable near-Infrared and Visible-Light Transmittance in Nanocrystal-in-Glass Composites. *Nature* **2013**, *500*, 323-326.

(3) Urban, J. J. Prospects for Thermoelectricity in Quantum Dot Hybrid Arrays. *Nat. Nanotechnol.* **2015**, *10*, 997-1001.

(4) Brus, L. E. A Simple Model for the Ionization Potential, Electron Affinity, and Aqueous Redox Potentials of Small Semiconductor Crystallites. *J. Chem. Phys.* **1983**, *79*, 5566-5571.

(5) Bawendi, M. G.; Steigerwald, M. L.; Brus, L. E. The Quantum-Mechanics of Larger Semiconductor Clusters (Quantum Dots). *Annu. Rev. Phys. Chem.* **1990,** *41*, 477-496.

(6) Heath, J. R.; Shiang, J. J. Covalency in Semiconductor Quantum Dots. *Chem. Soc. Rev.* **1998**, *27*, 65-71.

(7) Battaglia, D.; Peng, X. Formation of High Quality InP and InAs Nanocrystals in a Noncoordinating Solvent. *Nano Lett.* **2002**, *2*, 1027-1030.

(8) Liu, W.; Chang, A. Y.; Schaller, R. D.; Talapin, D. V. Colloidal InSb Nanocrystals. *J. Am. Chem. Soc.* **2012**, *134*, 20258-20261.

(9) Das, A.; Shamirian, A.; Snee, P. T. Arsenic Silylamide: An Effective Precursor for Arsenide Semiconductor Nanocrystal Synthesis. *Chem. Mater.* **2016**, *28*, 4058-4064.

(10) van Embden, J.; Latham, K.; Duffy, N. W.; Tachibana, Y. Near-Infrared Absorbing $Cu_{12}Sb_4S_{13}$ and $Cu_3SbS_4$ Nanocrystals: Synthesis, Characterization, and Photoelectrochemistry. *J. Am. Chem. Soc.* **2013**, *135*, 11562-11571.

(11) Guin, S. N.; Negi, D. S.; Datta, R.; Biswas, K. Nanostructuring, Carrier Engineering and Bond Anharmonicity Synergistically Boost the Thermoelectric Performance of p-type $AgSbSe_2$-ZnSe. *J. Mat. Chem. A* **2014**, *2*, 4324-4331.

(12) Nielsen, M. D.; Ozolins, V.; Heremans, J. P. Lone Pair Electrons Minimize Lattice Thermal Conductivity. *Energy Environ. Sci.* **2013,** *6*, 570-578.

(13) Morelli, D. T.; Jovovic, V.; Heremans, J. P. Intrinsically Minimal Thermal Conductivity in Cubic I-V-$VI_2$ Semiconductors. *Phys. Rev. Lett.* **2008**, *101*, 035901.

(14) Guin, S. N.; Srihari, V.; Biswas, K. Promising Thermoelectric Performance in n-type $AgBiSe_2$: Effect of Aliovalent Anion Doping. *J. Mat. Chem. A* **2015**, *3*, 648-655.

(15) Chen, C.; Qiu, X.; Ji, S.; Jia, C.; Ye, C. The Synthesis of Monodispersed $AgBiS_2$ Quantum Dots with a Giant Dielectric Constant. *CrystEngComm* **2013**, *15*, 7644-7648.

(16) Zhou, B.; Li, M.; Wu, Y.; Yang, C.; Zhang, W.-H.; Li, C. Monodisperse $AgSbS_2$ Nanocrystals: Size-Control Strategy, Large-Scale Synthesis, and Photoelectrochemistry. *Chem. Eur. J.* **2015**, *21*, 11143-11151.

(17) Liu, Y.; Cadavid, D.; Ibanez, M.; De Roo, J.; Ortega, S.; Dobrozhan, O.; V. Kovalenko, M.; Cabot, A. Colloidal $AgSbSe_2$ Nanocrystals: Surface Analysis, Electronic Doping and Processing into Thermoelectric Nanomaterials. *J. Mat. Chem. C* **2016**, *4*, 4756-4762.

(18) Gynane, M. J. S.; Hudson, A.; Lappert, M. F.; Power, P. P. Synthesis and Electron Spin Resonance Study of Stable Dialkyls and Diamides of Phosphorus and Arsenic, $R^1{}_2m\cdot$ and $(R^2{}_2N)_2M\cdot$. *J. Chem. Soc., Chem. Commun.* **1976**, 623-624.

(19) Gynane, M. J. S.; Hudson, A.; Lappert, M. F.; Power, P. P.; Goldwhite, H. Bulky Alkyls, Amides, and Aryloxides of Main Group 5 Elements. Part 1. Persistent Phosphinyl and Arsinyl Radicals ·MRR' and Their Chloroprecursors MRR'Cl and Related Compounds. *J. Chem. Soc., Dalton Trans.* **1980**, 2428-2433.

(20) Carmalt, C. J.; Compton, N. A.; Errington, R. J.; Fisher, G. A.; Moenandar, I.; Norman, N. C.; Whitmire, K. H., Homoleptic bismuth amides. In *Inorg. Synth.*, John Wiley & Sons, Inc.: 2007; pp 98-101.

(21) Bochmann, M.; Song, X.; Hursthouse, M. B.; Karaulov, A. Chalcogenolato Complexes of Bismuth and Antimony. Syntheses, Thermolysis Reactions, and Crystal Structure of $Sb(SC_6H_2Pr^i{}_3\text{-}2,4,6)_3$. *J. Chem. Soc., Dalton Trans.* **1995**, 1649-1652.

(22) Arudi, R. L.; Sutherland, M. W.; Bielski, B. H. J. Purification of Oleic Acid and Linoleic Acid. *J. Lipid. Res.* **1983,** *24*, 485-488.

(23) Becke, A. D. Density Functional Thermochemistry. 3. The Role of Exact Exchange. *J. Chem. Phys.* **1993,** *98*, 5648-5652.

(24) Lee, C. T.; Yang, W. T.; Parr, R. G. Development of the Colle-Salvetti Correlation Energy Formula into a Functional of the Electron Density. *Phys. Rev. B* **1988,** *37*, 785-789.

(25) Frisch, M. J.; Trucks, G. W.; Schlegel, H. B.; Scuseria, G. E.; Robb, M. A.; Cheeseman, J. R.; Scalmani, G.; Barone, V.; Mennucci, B.; Petersson, G. A.; Nakatsuji, H.; Caricato, M.; Li, X.; Hratchian, H. P.; Izmaylov, A. F.; Bloino, J.; Zheng, G.; Sonnenberg, J. L.; Hada, M.; Ehara, M.; Toyota, K.; Fukuda, R.; Hasegawa, J.; Ishida, M.; Nakajima, T.; Honda, Y.; Kitao, O.; Nakai, H.; Vreven, T.; Jr., J. A. M.; Peralta, J. E.; Ogliaro, F.; Bearpark, M.; Heyd, J. J.; Brothers, E.; Kudin, K. N.; Staroverov, V. N.; Kobayashi, R.; Normand, J.; Raghavachari, K.; Rendell, A.; Burant, J. C.; Iyengar, S. S.; Tomasi, J.; Cossi, M.; Rega, N.; Millam, J. M.; Klene, M.; Knox, J. E.; Cross, J. B.; Bakken, V.; Adamo, C.; Jaramillo, J.; Gomperts, R.; Stratmann, R. E.; Yazyev, O.; Austin, A. J.; Cammi, R.; Pomelli, C.; Ochterski, J. W.; Martin, R. L.; Morokuma, K.; Zakrzewski, V. G.; Voth,

G. A.; Salvador, P.; Dannenberg, J. J.; Dapprich, S.; Daniels, A. D.; Farkas, Ö.; Foresman, J. B.; Ortiz, J. V.; Cioslowski, J.; Fox, D. J. *Gaussian 09*, Revision E.01; Wallingford CT, 2009.
(26) Wadt, W. R.; Hay, P. J. *Ab Initio* Effective Core Potentials for Molecular Calculations - Potentials for Main Group Elements Na to Bi. *J. Chem. Phys.* **1985,** *82*, 284-298.
(27) Dennington, R.; Keith, T.; Millam, J. *Gaussview*, Semichem Inc.: Shawnee Mission, KS, 2009.
(28) Wojciechowski, K.; Tobola, J.; Schmidt, M.; Zybala, R. Crystal Structure, Electronic and Transport Properties of $AgSbSe_2$ and $AgSbTe_2$. *J. Phys. Chem. Solids* **2008,** *69*, 2748-2755.
(29) Guin, S. N.; Chatterjee, A.; Negi, D. S.; Datta, R.; Biswas, K. High Thermoelectric Performance in Tellurium Free p-type $AgSbSe_2$. *Energy Environ. Sci.* **2013**, *6*, 2603-2608.
(30) Garza, J. G.; Shaji, S.; Rodriguez, A. C.; Das Roy, T. K.; Krishnan, B. $AgSbSe_2$ and $AgSb(S,Se)_2$ Thin Films for Photovoltaic Applications. *Appl. Surf. Sci.* **2011**, *257*, 10834-10838.
(31) Soliman, H. S.; Abdel-Hady, D.; Ibrahim, E. Optical Properties of Thermally Vacuum Evaporated $AgSbSe_2$ Thin Films. *J. Phys.: Condens. Matter* **1998**, *10*, 847.
(32) Liu, Z.; Shuai, J.; Geng, H.; Mao, J.; Feng, Y.; Zhao, X.; Meng, X.; He, R.; Cai, W.; Sui, J. Contrasting the Role of Mg and Ba Doping on the Microstructure and Thermoelectric Properties of p-type $AgSbSe_2$. *ACS Appl. Mater. Interfaces* **2015**, *7*, 23047-23055.
(33) Xiao, C.; Qin, X.; Zhang, J.; An, R.; Xu, J.; Li, K.; Cao, B.; Yang, J.; Ye, B.; Xie, Y. High Thermoelectric and Reversible p-n-p Conduction Type Switching Integrated in Dimetal Chalcogenide. *J. Am. Chem. Soc.* **2012**, *134*, 18460-18466.
(34) Xiao, C.; Xu, J.; Cao, B.; Li, K.; Kong, M.; Xie, Y. Solid-Solutioned Homojunction Nanoplates with Disordered Lattice: A Promising Approach toward "Phonon Glass Electron Crystal" Thermoelectric Materials. *J. Am. Chem. Soc.* **2012**, *134*, 7971-7977.
(35) Kang, M. S.; Sahu, A.; Norris, D. J.; Frisbie, C. D. Size-Dependent Electrical Transport in CdSe Nanocrystal Thin Films. *Nano Lett.* **2010**, *10*, 3727-3732.

$AgSbSe_2$ and $AgBiSe_2$ have potential applications for alternative energy generation. We demonstrated the colloidal syntheses of dimetal chalcogenide nanomaterials with good crystallinity and size distributions. Current-voltage measurements reveal Ohmic contact behavior, which indicates efficacy in electronic devices.

Insert Table of Contents artwork here